First results from a Liquid Argon Time Projection Chamber in a Magnetic Field

A. Badertscher, M. Laffranchi, A. Meregaglia, A. Müller, A. Rubbia

Institute for Particle Physics, ETH Hönggerberg, CH-8093 Zürich, Switzerland

Abstract

A small liquid argon Time Projection Chamber (LAr TPC) was operated for the first time in a magnetic field of 0.55 Tesla. The imaging properties of the detector were not affected by the magnetic field. In a test run with cosmic rays a sample of through going and stopping muons was collected. The chamber with the readout electronics and the experimental setup are described. A few selected events were reconstructed and analyzed and the results are presented.

The magnetic bending of the charged particle tracks allows the determination of the electric charge and the momentum, even for particles not fully contained in the drift chamber. These features are e.g. required for future neutrino detectors at a neutrino factory.

Key words: Liquid argon, Time Projection Chamber, Calorimeter, Magnetic Spectrometer, Neutrino Detectors, Neutrino Factories
PACS: 29.30.Aj, 29.40.Gx, 29.40.Vj, 34.50.Bw

1 Introduction

1.1 The liquid argon Time Projection Chamber

The liquid argon time projection chamber (LAr TPC) was proposed by C. Rubbia in 1977 [1]. With an extensive R&D program, including the construction of several prototypes of increasing mass, the ICARUS collaboration [2] has demonstrated the feasibility of this novel technology for large mass detectors. A 600 ton (T600) module consisting of two identical 300 ton half-modules was built and successfully tested [3].
The LAr TPC is a 3-dimensional homogeneous tracking device with excellent, high resolution imaging properties, and, at the same time it is a fine grain

calorimeter for fully contained particles due to the measurement of the energy loss dE/dx along the charged particle tracks. The detector is ideally suited for neutrino physics and a sensitive search for nucleon decays [4]. In ultra-pure LAr (contamination < 0.1 ppb O_2 equivalent) the ionization charge of a track can be drifted undistorted over a distance of the order of meters in a uniform electric field.

Figure 1 shows a schematic view of a TPC; it consists of a cathode, the sen-

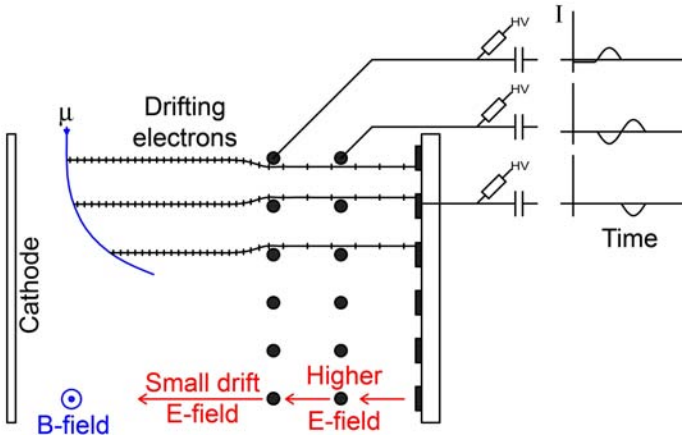

Figure 1. Schematic view of a TPC in a magnetic field. A charged particle is passing through an ionization medium (e.g. LAr) and the electrons drift along the electric field lines to the sensors.

sor planes and field shaping electrodes (not shown in the figure) to produce a homogeneous drift field. The ionization electrons drift along the electric drift field to the sensor planes, where the charge is measured. In the LAr TPC described here there are three sensor planes: the first two planes are multi-wire proportional chambers and the third plane is a printed circuit board (PCB) with conducting strips. Preliminary results obtained with this chamber were published in [5] and a detailed description is given in [6]. The sensor planes are biased with potentials, such, that the wire chambers are transparent to the drifting electrons, they only pick up an induced signal from the electrons passing through the plane (induction planes), the electrons are then collected on the strips of the third plane (collection plane). Each plane provides a two-dimensional projection of a track with the number of the hit wire (strip) and the drift time as coordinates. The t_0 for the drift time is given by trigger counters. The drift distance is calculated from the measured drift time and the known drift velocity v_d. Combining the wire hits of equal drift time from at least two planes allows the three–dimensional reconstruction of a track [3,7].

As a consequence of the short mean free path of the drifting electrons in LAr, they do not gain enough kinetic energy between collisions to ionize other atoms, thus, there is no charge multiplication at the wires in LAr. However, the high ionization density in the liquid allows a direct measurement of the ionization charge with a very low noise amplifier; the expected charge for a

minimum ionizing particle (mip) is of the order of 13 000 electrons for 2 mm track length (at a drift field of 0.5 kV/cm). The commercial VME–like CAEN modules [1], designed and built for the ICARUS experiment (see chapter 3), have been used as front end electronics.
The low drift velocity (1.6 mm/μs at a drift field of 0.5 kV/cm) and the long drift paths in detectors with big sensitive volumes (as e.g. in ICARUS) implies that the electrons spend a long time in liquid argon. This leads to the requirement of an extremely low concentration of electronegative impurities (as e.g. oxygen) in LAr because the drifting electrons can be captured by electronegative atoms or molecules, decreasing the charge arriving at the sensors. If the impurity concentration is constant over the whole volume, the charge decreases exponentially with the drift time:

$$Q(t) = Q(t_0)\, e^{-\frac{t}{\tau}} \tag{1}$$

where τ is the mean lifetime of the electrons in argon. The lifetime is directly connected to the O_2 equivalent impurity concentration ρ by an inverse linear relationship [8]:

$$\tau[\mu\mathrm{s}] \approx \frac{300}{\rho[ppb]} \tag{2}$$

The commercial LAr 48 is specified to 1 ppm; this corresponds to a mean lifetime of only 0.3 μs, absolutely insufficient for a TPC. A considerable amount of R&D has been performed by the ICARUS collaboration in order to master the argon purification process [3,9].
The drift velocity of the electrons in liquid argon is small compared to the thermal velocity as a result of frequent collisions of the electrons with the argon atoms; it can be approximated by [10]

$$v_d = \frac{e}{2m} \cdot E \cdot \tau_c, \tag{3}$$

where τ_c is the mean time between collisions. The drift velocity has been measured at different temperatures as a function of the drift field, and was fitted to an empirical formula [11]. For later use (see chapter 1.2) we introduce here the mobility of the electrons, defined as [10]:

$$\mu \equiv \frac{v_d}{E} \tag{4}$$

Except for very low E-fields, the electron mobility is not constant. With equa-

[1] www.caen.it

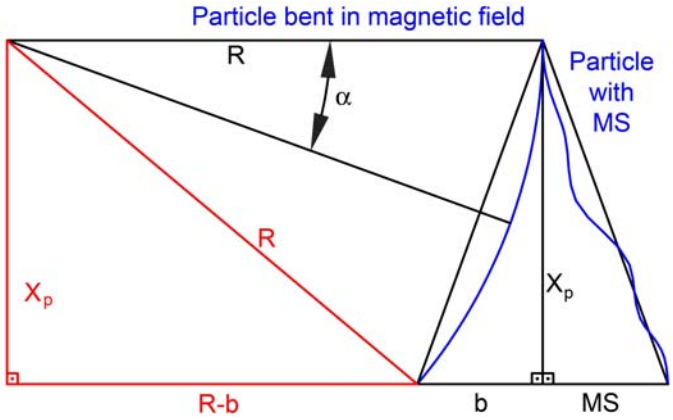

Figure 2. Definition of the bending parameter b of a particle, where x_b is the thickness of the particle trajectory projected into the bending plane, and R is the bending radius.

tion 3, we find for the mobility:

$$\mu = \frac{e}{2m} \cdot \tau_c \tag{5}$$

1.2 The LAr TPC in a magnetic field

The possibility to complement the features of the LAr TPC with those provided by a magnetic field has been considered and would open new possibilities [5,12,13,14]: (a) charge discrimination, (b) momentum measurement of particles escaping the detector (e.g. high energy muons), (c) very precise kinematics, since the measurement precision is limited by multiple scattering (e.g. $\Delta p/p$ 4% for a track length of $L = 12\,\mathrm{m}$ and a field of $B = 1\,\mathrm{Tesla}$). The challenging possibility to magnetize a very large, multi–kton, volume of argon has been addressed in [15].
The orientation of the magnetic field can be chosen such, that the bending direction is in the direction of the drift where the best spatial resolution is achieved. This is possible since the Lorentz angle is small, as is shown below. However, it is not mandatory and the B–field could also be parallel to the drift field. In the following we consider the case where the magnetic field is perpendicular to the electric drift field.
The required magnetic field for charge discrimination for a thickness x in LAr (x_p is the projected thickness into the bending plane) is given by the bending parameter b [13], as defined in Figure 2:

$$b^2 - 2Rb + x_p^2 = 0 \tag{6}$$

Neglecting the b^2 term for $\alpha \ll 1$, b can be approximated by:

$$b \approx \frac{x_p^2}{2R} \tag{7}$$

The radius of curvature R of the charged track due to the magnetic field is given by:

$$R = \frac{p_t}{(0.3\,B)} \tag{8}$$

where B is the magnetic field strength, p_t is the transverse momentum, i.e. $p_t = p \cdot \cos\lambda$, and λ is the angle between the track and its projection on the bending plane (pitch angle). Thus, the bending becomes:

$$b \approx \frac{x_p^2}{2R} = \frac{0.3\,B(Tesla)(x_p(m))^2}{2p_t(GeV)} = \frac{0.3\,B(Tesla)(x(m))^2\,\cos\lambda}{2p(GeV)} \tag{9}$$

The multiple scattering contribution to b can be obtained from [16, eq. 27.10]. Neglecting the logarithmic correction, inserting $X_0 = 14\,\mathrm{cm}$ as radiation length of liquid argon and using the projected deviation $MS = x\theta_0/\sqrt{3}$ (see also Figure 2), one obtains:

$$MS \approx \frac{0.02\,(x(m))^{3/2}}{p(GeV)} = \frac{0.02\,(x_p(m))^{3/2}}{p_t(GeV)\sqrt{\cos\lambda}} \tag{10}$$

The momentum resolution of a particle bending in a uniform magnetic field can be found from equation 8. With the introduction of the curvature, defined as $k \equiv 1/R$, it becomes:

$$\frac{\Delta p}{p} = \frac{p\,\Delta k\,\cos\lambda}{0.3\,B} \tag{11}$$

At low momenta, we can safely neglect the contribution from the position measurement error given the readout pitch and drift time resolution and use the [16, eq. 28.44] for the Δk due to the multiple scattering. The momentum resolution is then given by

$$\frac{\Delta p}{p} \approx \frac{0.14}{B(Tesla)\sqrt{(x(m))\,\cos\lambda}} = \frac{0.14}{B(Tesla)\sqrt{(x_p(m))\,\cos\lambda}} \tag{12}$$

and the statistical significance for charge separation can be written as ($b^{\pm}$ are the bending for positive and negative charges):

$$\sigma \approx \frac{b^+ - b^-}{MS} \approx \frac{2b}{MS} \approx 15\, B(Tesla)\sqrt{x(m)\ \cos^3\lambda} \tag{13}$$

For example, with a field of 0.55 T, the charge of tracks of 10 cm length can be separated at $2.6\,\sigma$ with $\lambda = 0$. The requirement for a 3σ charge discrimination can be written as $b^+ - b^- = 2b > 3\,\mathrm{MS}$, which implies a field strength of

$$B \geq \frac{0.2\,(Tesla)}{\sqrt{x(m)\ \cos^3\lambda}} \tag{14}$$

For long penetrating tracks like muons, a field of 0.1 T allows to discriminate the charge for tracks longer than 4 m, if perpendicular to the magnetic field. This corresponds for example to a muon momentum threshold of 800 MeV/c. Unlike muons or hadrons, the early showering of electrons makes their charge identification difficult. The track-length usable for charge discrimination is limited to a few radiation lengths after which the showers make the recognition of the parent electron more difficult. In practice, charge discrimination is possible for high fields $x = 1X_0 \rightarrow B > 0.5$ Tesla, $x = 2X_0 \rightarrow B > 0.4$ Tesla, $x = 3X_0 \rightarrow B > 0.3$ Tesla. From simulations, we found that the determination of the charge of electrons of energy in the range between 1 and 5 GeV is feasible with good purity, provided the field has a strength in the range of 1 T. Preliminary estimates show that these electrons exhibit an average curvature sufficient to have electron charge discrimination with an efficiency of 20 % for a contamination with the wrong charge of less than 1 % [14].

In the presence of a magnetic field a Lorentz force is acting on each moving charge, modifying the drift properties of the electrons. As a consequence, the electrons will not move along the electric field lines, but on a straight line at an angle α to the E–field. In general, the drift velocity in a static electromagnetic field is given by [16, eq. 24.7]:

$$\overrightarrow{v}_{DB} = \frac{v_d}{1+\omega^2\tau_c^2}[\widehat{E} + \omega\tau_c(\widehat{E} \wedge \widehat{B}) + \omega^2\tau_c^2(\widehat{E}\cdot\widehat{B})\widehat{B}] \tag{15}$$

where $\widehat{E}$ is the unit vector in the E–field direction, $\widehat{B}$ the unit vector in the B–field direction and ω is the cyclotron frequency:

$$\omega = \frac{e \cdot B}{m} \tag{16}$$

In the case that the electric and magnetic fields are perpendicular to each other, the electrons will drift along a straight line at an angle α with respect

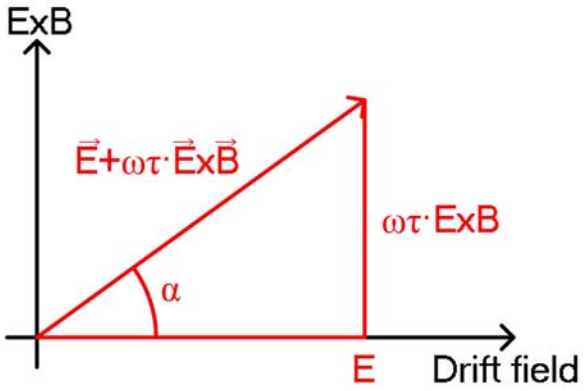

Figure 3. Definition of the Lorentz angle α (for perpendicular E– and B–fields).

to the electric field lines (see Figure 3). In this case equation 15 is simplified to:

$$\overrightarrow{v}_{DB} = \frac{v_d}{1+\omega^2\tau_c^2}[\hat{E} + \omega\tau_c(\hat{E} \wedge \hat{B})] \tag{17}$$

From Figure 3 it can be seen that for the case of perpendicular E– and B–fields the Lorentz angle α is given by:

$$\tan\alpha = \omega\tau_c \tag{18}$$

From equation 5 we obtain for τ_c:

$$\tau_c = \mu \cdot \frac{2m}{e} \tag{19}$$

With the definition of the mobility in equation 5 and using the empirical expression for the drift velocity [11], we can calculate the Lorentz angle for a given magnetic field (for perpendicular E– and B–fields):

$$\tan\alpha = \frac{e \cdot B}{m} \cdot \mu \cdot \frac{2m}{e} = 2\mu B \tag{20}$$

The Lorentz angle is expected to be very small in the liquid, e.g. 1.7° at $E = 500\,\mathrm{V/cm^{-1}}$ and $B = 0.5\,\mathrm{T}$. Embedding the volume of argon into a magnetic field should therefore not alter the imaging properties of the detector and the measurement of the bending of charged hadrons or penetrating muons would allow a precise determination of the momentum and a determination of their charge.

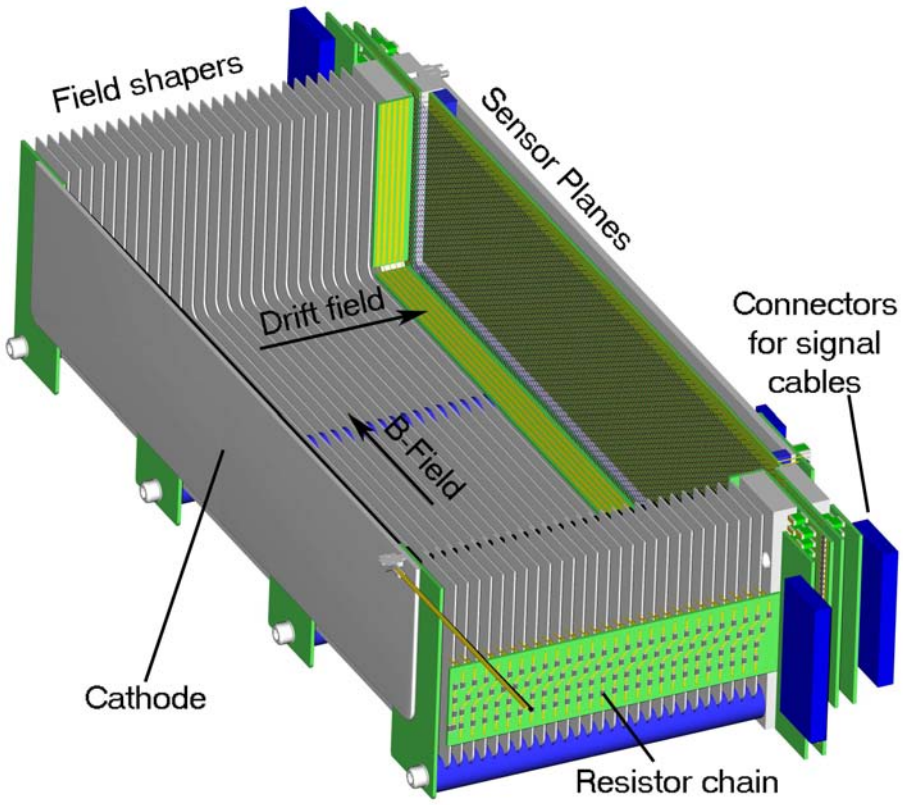

Figure 4. Cut view into the open drift chamber.

2 TPC construction

2.1 Overview

The dimensions of the cryostat and the chamber were chosen to fit into the recycled SINDRUM I magnet [2]. The sensitive volume of the chamber has a length (in the direction of the solenoid axis) of 300 mm, a height of 150 mm and a width corresponding to a maximal drift length of 150 mm.
The drift chamber (see Figure 4) consists of a rectangular cathode, 27 field shaping electrodes equally distributed over the whole drift path and three detector planes. The first two detector planes are wire chambers with the wires oriented at $\pm 60^\circ$ to the vertical; the 127 stainless steel wires for each plane have a diameter of 100 μm and a pitch of 2 mm. The third plane is a PCB with horizontal strips with a width of 1 mm and a pitch of 2 mm on which the drift electrons are collected. The potentials of the three planes can be varied from outside; the wires and the strips are coupled through a 470 MΩ resistor to the bias high voltage and a 1.4 pF capacitor to 3 m long twisted

[2] The magnet was kindly lent to us by the Paul Scherrer Institute (PSI), CH-5232 Villigen, Switzerland.

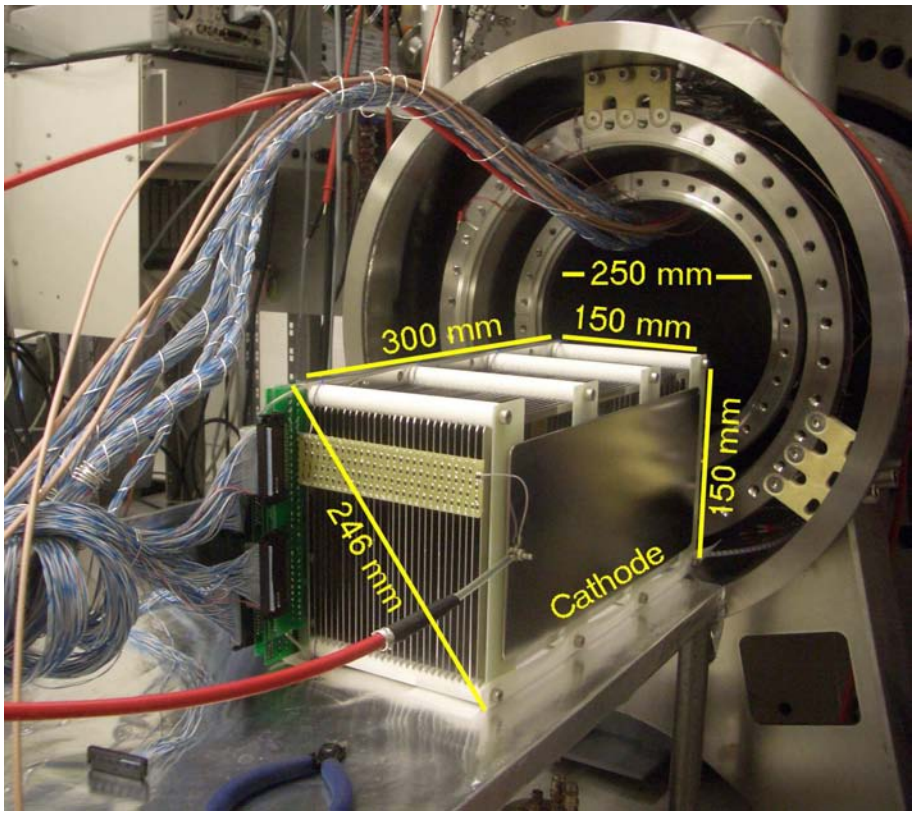

Figure 5. The liquid argon time projection chamber ready to slide into the cryostat.

pair cables (see chapter 3), which are connected to the feedthroughs at the warm part of the cryostat.
The cathode and the field shaping electrodes are designed to hold the high voltage (up to a maximum of 22.5 kV was applied) and are thus carefully insulated with PCBs and Macor™ rods. Eight Macor rods with a diameter of 15 mm at the bottom and the top of the chamber were used to assemble the cathode, the field shaping electrodes and the the sensor planes (see Figure 5), giving enough mechanical stability to the chamber. With a resistor chain, connected to the cathode HV at one end and to the wire chambers at the other end, the field shaping electrodes are connected to the appropriate potential, in order to obtain a homogeneous drift field in the whole chamber volume. Figure 5 shows the assembled chamber ready to slide into the cryostat.

The chamber is oriented in the LAr vessel such, that the drift direction is horizontal; the $\vec{E}$–field is perpendicular to the $\vec{B}$–field, which is also horizontal. This orientation of the chamber has the advantage that the bending of the charged particles incident from the top is in the drift direction, where the spatial resolution is best.
Table 1 summarizes the most important chamber parameters.

Total volume	$400\,mm \times 170\,mm \times 170\,mm$
Sensitive volume	$300\,mm \times 150\,mm \times 152.9\,mm$
Sensing planes	1^{st} Induction
	2^{nd} Induction
	Collection
Induction planes	wires at $\pm 60°$ to the vertical
	127 wires per plane
	$2\,mm$ pitch
	$-200\,V$ bias voltage of 1^{st} induction plane
	$0\,V$ bias voltage of 2^{nd} induction plane
	$2.8\,mm$ distance between 1^{st} and 2^{nd} induction plane
Collection plane	1 mm wide copper strips on a printed circuit board
	75 strips (channels)
	$2\,mm$ pitch
	$+280\,V$ bias voltage
	$3.1\,mm$ distance between 2^{nd} induction plane and strips
Electronic channels	$127 + 127 + 75 = 329$
Electric drift field	$0 < E < 2\,kV/cm$
Expected charge for a mip (μ)	$\sim 13\,000$ electrons for 2 mm track length at $0.5\,kV/cm$

Table 1
Summary of the chamber parameters

2.2 The sensing planes

The induction planes are composed of a robust frame made of non-magnetic stainless steel (316L) with inner dimensions of 302 mm × 152 mm (outer dimensions: 360 mm × 194 mm). The frame thickness of the first induction plane is 10 mm and for for the second induction plane it is 8 mm; it was calculated to avoid a deformation of the frames under the force of the wires. Each plane has 127 wires and each wire has a tension (at room temperature) of (0.75 ± 0.03) N; the distance between the two wire planes was set to 2.8 mm with a plastic spacer. The PCBs to solder the wires, the coupling capacitors and the resistors were glued to the steel frame with Araldite™. The 100 μm wires are made of the same material as the frames (steel 316L); they were strung and soldered at PSI.

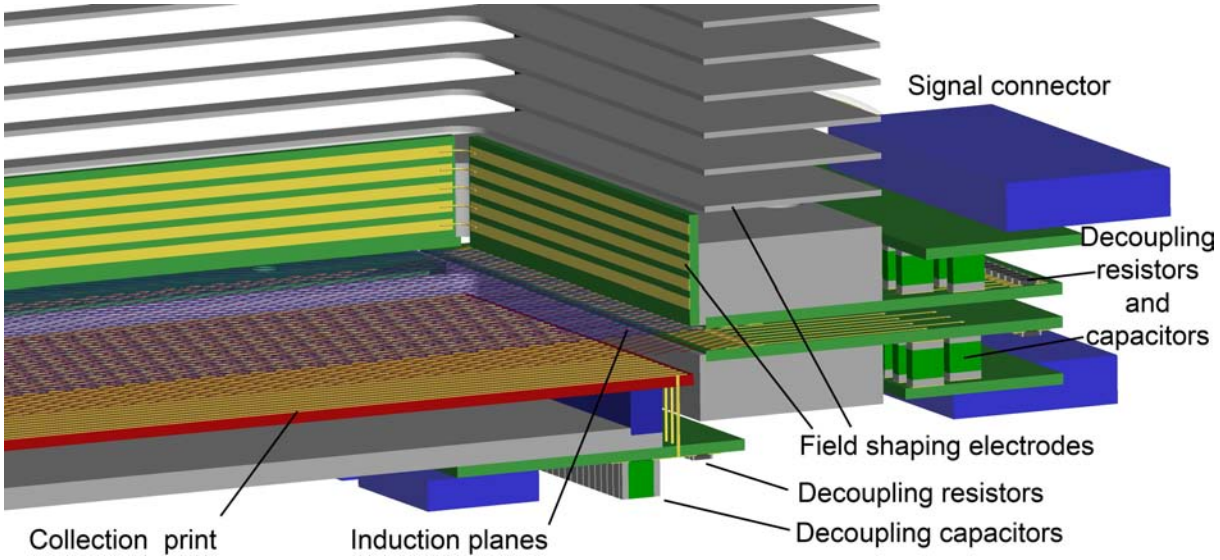

Figure 6. Zoomed view of the three sensing planes with the signal decoupling prints.

The coupling capacitors and resistors are mounted on the same PCB with the wires (see Figure 6). The connectors for the signal cables are on a separate PCB, connected through the coupling capacitors.
The collection plane is a PCB with a size of 300 mm × 150 mm in order to fit inside the frame of the second induction plane. On the PCB there are 75 strips, 1 mm wide and with a pitch of 2 mm. On the back side of the PCB a 2 mm thick steel plate is mounted at a distance of 5 mm from the PCB. The steel plate and the PCB are glued to the Macor bars. The steel plate is connected to ground; it stabilizes mechanically the chamber and shields the collection plane. The PCB with the coupling resistors, capacitors and the signal connectors is glued to the bottom side of the steel plate; the strips are connected with copper wires to the PCB. Figure 6 shows a zoomed view of the chamber with the assembled sensing planes and the position of the coupling resistors and capacitors.
Tests were made to prove that the glued PCBs do not detach from the frames and the capacitors do not break due to the mechanical stress during the cooling down: the chamber (without cathode and field shaping electrodes) was cooled down as quickly as possible, but avoiding excessive thermal stress. For a cooling down time of about 10 hours, the maximal temperature difference between the frame and the surrounding temperature was about 4 °C. This value for the maximal temperature difference was kept as a limit during the cooling down of the whole chamber in the cryostat.

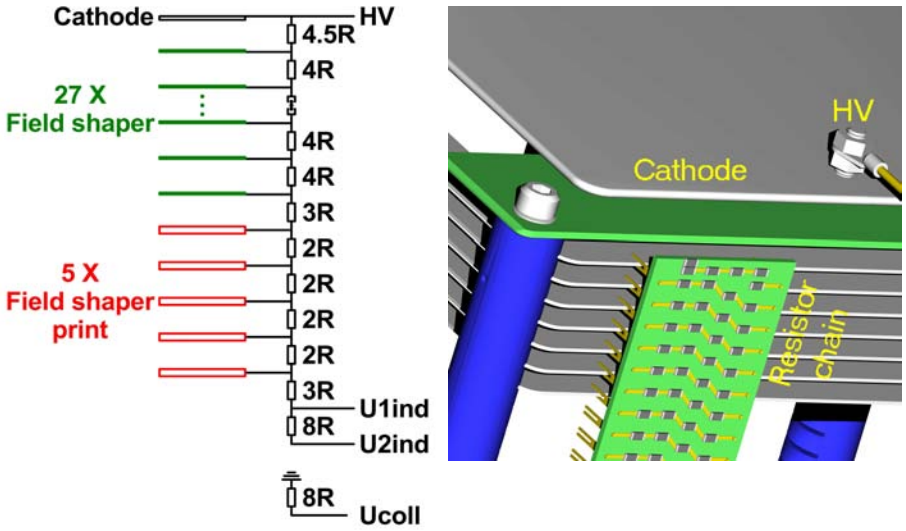

Figure 7. (left) Scheme of the resistor chain for the field shaping electrodes. (right) CAD drawing of the resistor chain connected to the field shaping electrodes.

2.3 The cathode and the field shaping electrodes

The cathode is a 2 mm thick stainless steel plate connected to the high voltage and to the resistor chain for the field shaping electrodes. The plate is big enough not to distort the field in the drift volume near the cathode; it is insulated by a minimal distance of 20 mm to the LAr vessel, which is grounded. This distance is enough for liquid argon, which has a breakdown field strength of about $1.1-1.4\,\mathrm{MV/cm}$, depending on the purity of the argon.
The field shaping electrodes are made of 27 stainless steel (316L) frames, 0.8 mm thick, and surround the chamber volume. They are held at a distance of 5 mm by slits in the Macor™ rods. The field shaping electrodes are connected to a resistor chain from the high voltage to the wire chambers. The resistors are surface mounted metal film resistors with a nominal value (at room temperature) of $1\,\mathrm{G\Omega}$. Figure 7 (left) shows the electric scheme of the resistor chain; the resistance between two field shaping electrodes is called 4R ($\mathrm{R} = 1\,\mathrm{G\Omega}$). The distance between the first induction plane and the closest field shaping electrode is 16 mm. To avoid a distortion of the drift field near the edge of this first wire plane, a PCB with strips (see Figure 6) was glued to the inner sides of the 10 mm thick wire frame and the strips were also connected to the resistor chain; the resistance between the the first field shaping electrode and the first strip is 3R, and between strips it is 2R. Figure 7 (right) shows how the resistor chain is connected through gold plated pins to the field shaping electrodes. The total resistance of the resistor chain is more than $100\,\mathrm{G\Omega}$ and the current is negligible. The resistors used for the chain were tested to withstand shock cooling in $\mathrm{LN_2}$, since they were all connected in series, hence, if one would break, there would be no drift field.

The sensing planes are put at such a potential that the wire chambers are transparent for the drifting electrons and then collected on the collection plane. With a wire diameter of 100 μm and a pitch of 2 mm, the fields before (E_1) and after (E_2) the plane have to fulfill the relation $E_2 > 1.37 \cdot E_1$ in order that the wire plane is 100 % transparent [6].
During the test of the chamber different bias voltages were tested to increase the signal to noise ratio; the planes were finally put to -200 V for the first induction, 0 V for the second induction and $+280$ V for the collection plane, with a drift field of 300 V/cm. This configuration corresponds to a field ratio of 2.3 through the first induction, and a ratio of 1.40 through the second induction plane.
The potentials are set externally by a VME HV power supply [3] with a declared ripple of less than 2 mV_{pp}. The potentials were fed into the cryostat through 2×20 kV SHV feedthroughs on a CF40 flange. The second induction plane has a 5 kV SHV connector and it is closed with a shortcut connector to the ground. The feedthroughs are connected to the chamber by 3 m long coaxial cables (type RG58).
The cathode is supplied by a high voltage power supply [4] with a declared ripple of less than $1 \cdot 10^{-5}$ or 10 mV_{pp}. Since the argon gas has a low dielectric strength, the connection of the HV feedthrough to the HV cable inside the argon container has been poured with Araldite™. During the test with cosmic ray muons the voltage of the cathode was first set to 22.5 kV. After one week of operation breakthroughs occurred. From that point on, the maximal voltage held was only 4.7 kV, corresponding to a drift field of 300 V/cm.

3 The readout electronics and the data acquisition system

3.1 The front–end electronics

The readout electronics works as a multichannel wave form digitizer for the 329 channels from the two induction planes and the collection plane. The V791 modules [17] developed for the ICARUS experiment together with CAEN were used as front–end electronics. Each channel is equipped with a low–noise current integrating preamplifier [18] followed by a Flash ADC with 10 bit resolution. All channels are sampled with a rate of 2.5 MHz, i.e., every 400 ns. The digitized data are continuously stored in a circular buffer, which is large

[3] ISEG type VHQ 205L 2×5 kV / 1 mA
[4] AIP WILD AG, type HCN 35–35000, 35 kV/1 mA

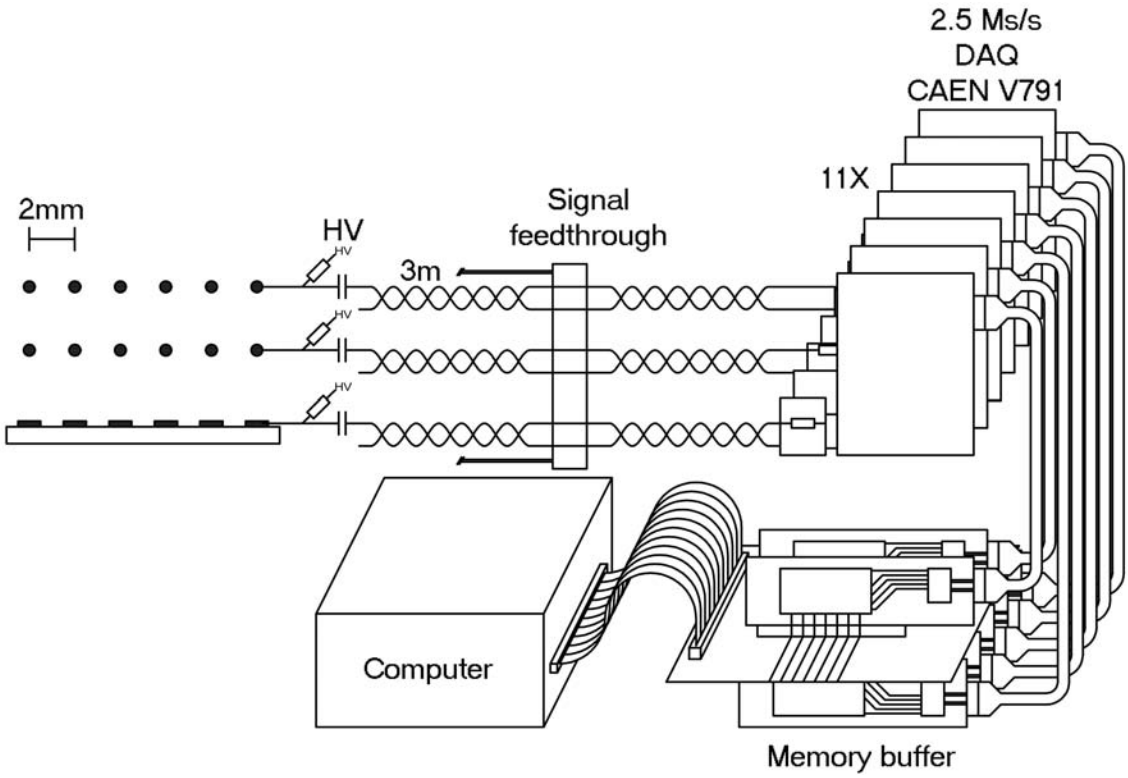

Figure 8. Block diagram of the data acquisition system.

enough to contain the data of all channels for a time interval of about 1 ms; the maximal drift time (t_{dmax}) occuring during this experiment was only about 150 μs. Figure 8 shows a schematic view of the data acquisition system. When a trigger occurs, the filling of the buffer continues for at least t_{dmax}, in order to have all the samples of the event stored in the buffer. Before the next trigger is accepted, all the data in the buffer are transferred to a PCI computer card in a PC; the PCI card is read out with a LabView™ program and the data stored on the hard disk.

The signal with a charge corresponding to about 13 000 electrons is decoupled from the high voltage by a surface mounted 470 MΩ resistor and a ceramic capacitor of 1.2 nF (large compared to the input wire plus cable capacity of about 130 pF). The chamber and the vacuum feedthroughs are connected by 3 m long twisted pair flat cables. The twisted pair cables are Teflon insulated [5] and are suited to use in vacuum and in high purity liquid argon. The low capacity twisted pair cable also suppresses possible microphonic noise due to vibrations in the magnetic field.

Outside the cryostat about 20 cm of the same type of twisted pair cables connect the feedthroughs to the front–end electronics. The signal cables are connected to the back plane of a VME crate containing the CAEN V791 modules with the preamplifiers and the ADCs. One module has 32 input channels. Its

[5] Amphenol, type 425-3016-068, CERN catalogue 04.21.21.368.5

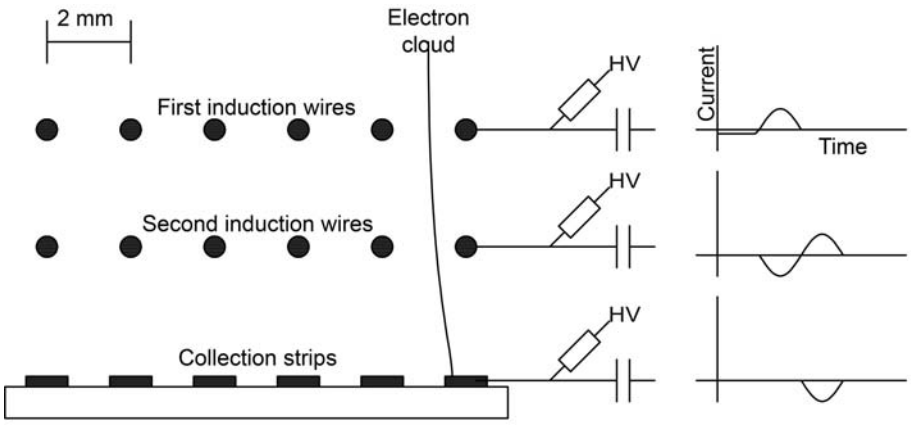

Figure 9. Schematic view of the pulse shapes for the three sensor planes.

function is to amplify, shape and digitize the signals coming from the detector and transmit the digitized data via a fast serial link to the buffer module. Two different versions of the V791 module are available, the Mod. V791C and the Mod. V791Q, which operate in "quasi current" and "quasi charge" mode, respectively; the two versions differ in the feed back and restore time constants. Figure 9 shows schematically the pulse shapes before the amplifier/shaper stage for the three sensor planes; the current mode is used for the unipolar signals from the first induction and the collection plane, and the charge mode is used for the middle plane (second induction plane). The measured signals are induced by the moving charge of the drift electrons and are proportional to the drift velocity. Thus, strictly speaking the signal from the first induction plane is also bipolar: a small negative part from the slowly drifting electrons approaching the plane from the drift volume, and a much larger positive part induced when the electrons have passed through the plane and drift away much faster in the larger drift field between the two induction planes. The bipolar signal of the middle plane is caused by the electron cloud, which is first approaching and then moving away from the plane. The collection plane, of course, produces a true unipolar signal.
The digitized data are converted[6] into three LDVS (Low Voltage Differential Signaling) data streams and continuously sent to a specially built interface with a circular buffer. At a clock frequency of 40 MHz, the following 21 bits of TTL data are transmitted with every clock cycle:

- 10–bit ADC data of the channels k;
- 10–bit ADC data of the channels $k+16$;
- 1 SYNC–bit, set to 11 when the ADC data of channels 15 (k = 15) and 31 are transmitted and 0 otherwise.

[6] National Semiconductor type DS90CR213

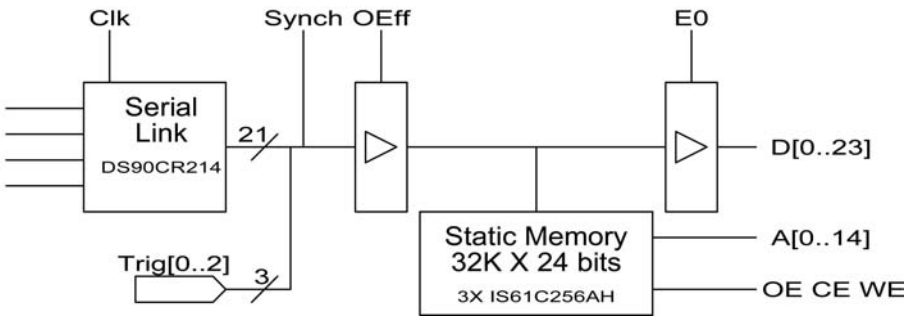

Figure 10. Schematic of the memory buffer card.

3.2 The buffer module

An interface between the eleven V791 CAEN cards and the computer has been built, able to store the continuous flow of digital data in a circular buffer and to send the data to the PCI card in the computer, once a trigger has occurred [6]. The interface consists of eleven buffer cards (one per V791 module) connected through a dedicated bus to the main board.
Figure 10 shows of the block diagram of the buffer card. A single buffer card contains a serial link receiver circuit (DS90CR214 of National Semiconductor) to convert the LVDS data streams from a V791 module back to 21 bits of CMOS/TTL data. As long as no trigger is detected, the data are stored into the memory. The buffer on each card has a size of $32\,\mathrm{k} \times 24$ bits. The two 10–bit data samples plus the synchronization bit transmitted in a cycle can hence be stored in a single memory cell; there are 3 bits left to store additional information, e.g. about the trigger. The size of the memory is large enough to store 2048 samples of a single channel. The address of the memory is generated by the main board, using an increment on every clock cycle and is the same for all the buffer cards. The address is coded with the Gray method [19] in order to reduce the signal interference on the bus.
The main board consists of a bus with slots for 19 buffer cards, two ALTERA FPGA (Field Programmable Gate Array) chips and an independent static memory of $2\times 512\,\mathrm{k}\times 16\,\mathrm{bit}$ [7]. One ALTERA chip (the EPM3128ATC100-5) is programmed to drive all the buffer cards during the waiting for a trigger and also handles the trigger [6]. After a trigger is detected, the EPM3128ATC100-5 chip waits a certain number of clock counts, which can be selected by a 5 dip–switch, and then stops the memory filling of all buffer cards in order to read the whole memory and send it to the computer. Choosing with the switch an appropriate waiting time to stop the memory filling after a trigger allows to set the length of the pre–trigger data, which are stored with an event. This is important for the fit of the base–line of a channel in the time before the actual signal starts. In our experiment with cosmic rays the switch was set so that the trigger time corresponded to the memory address 1024, i.e. the

[7] ISSI, type IS61LV51216

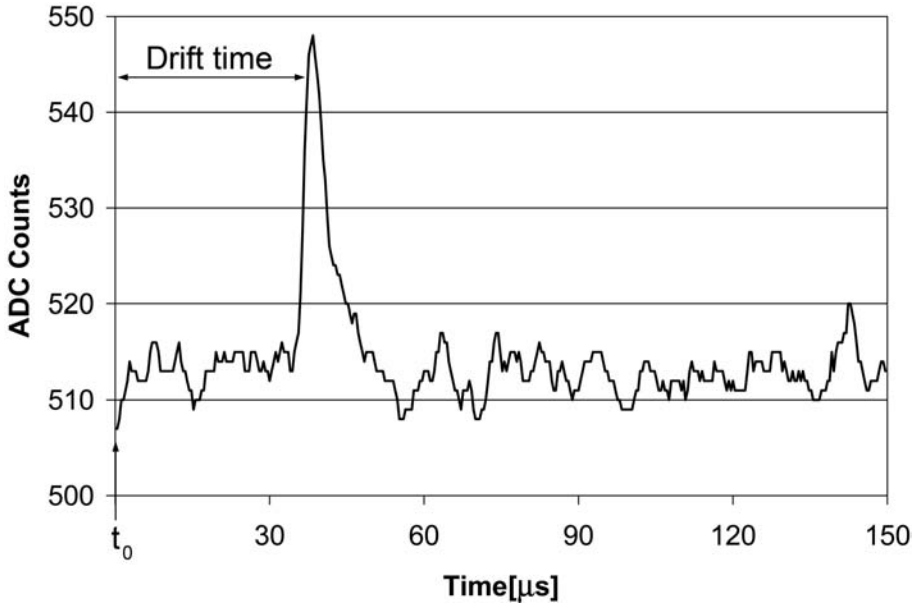

Figure 11. Raw data signal from the collection plane; t_0 indicates the trigger time.

middle of the buffer. Thus, half of the data stored as an event are pre–trigger data.

Figure 11 shows a stored signal from the collection plane with the trigger position and the drift time indicated.
When the memory of the buffer card 0 is completely read, the memory of the next buffer card is read. The data are transmitted to the second ALTERA chip, the EPM3256ATC144-7, and then to the computer via a PCI card. The second ALTERA EPM3256ATC144-7 is connected with a 16×1 Mbits memory and could be programmed to make a first data compression. In our experiment with the cosmic rays the ALTERA chip was only programmed to transmit the data from the buffer card to the PCI computer card.
A LabView™ program running under Windows XP on a PC read the data from the 12 MB/s PCI-7200™ from ADLink [8] and stored them in a file on the hard disk; 100 events were stored in a 137 MB file. The LabView program also has the option to display online the signals of each event, but this feature was normally deactivated during the data taking with cosmic rays, reducing the dead time for the next trigger. The maximal trigger rate was in this case about 1/2 Hz, corresponding to a data flow of about 685 kB/s.

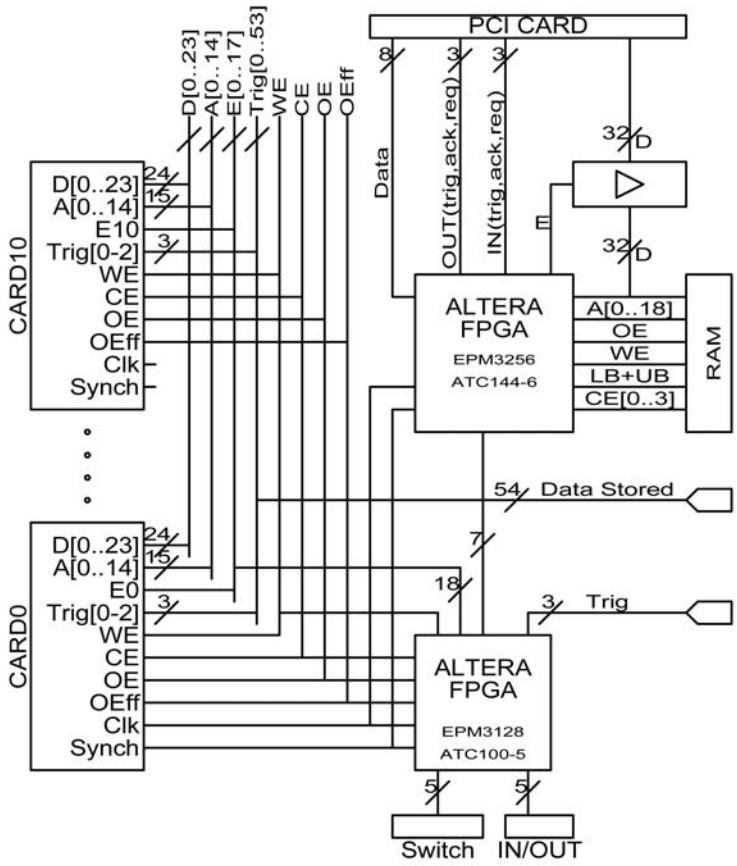

Figure 12. Schematic of the buffer module.

4 The experimental setup

The dimensions of the chamber and the LAr cryostat are such, that they fit into the bore hole of the recycled SINDRUM I magnet from PSI. Figure 13 is a 3D CAD drawing showing a cut through the setup with the essential components of the experiment.
The cryostat consists of three cylindrical stainless steel vessels (see section 4.1). The LAr vessel is shown in red and contains the chamber and the purified liquid argon. The LAr is kept in a liquid nitrogen (LN_2) bath to stabilize its temperature and pressure. The nitrogen bath, shown in blue, contains nitrogen with an absolute pressure of about 2.7 bar in order not to freeze out the argon, which is at about 1 bar. The outer most container for the vacuum insulation of the cryostat is shown in green in Figure 13.
The solenoid magnet can generate an axial magnetic field up to 0.55 T in the region of the chamber (see section 4.2). The magnet is cooled with a closed water cooling system connected to the main laboratory water cooling circuit. Eleven plastic scintillator counters are mounted on top, in the bore hole and

[8] ADLink Technology Inc.

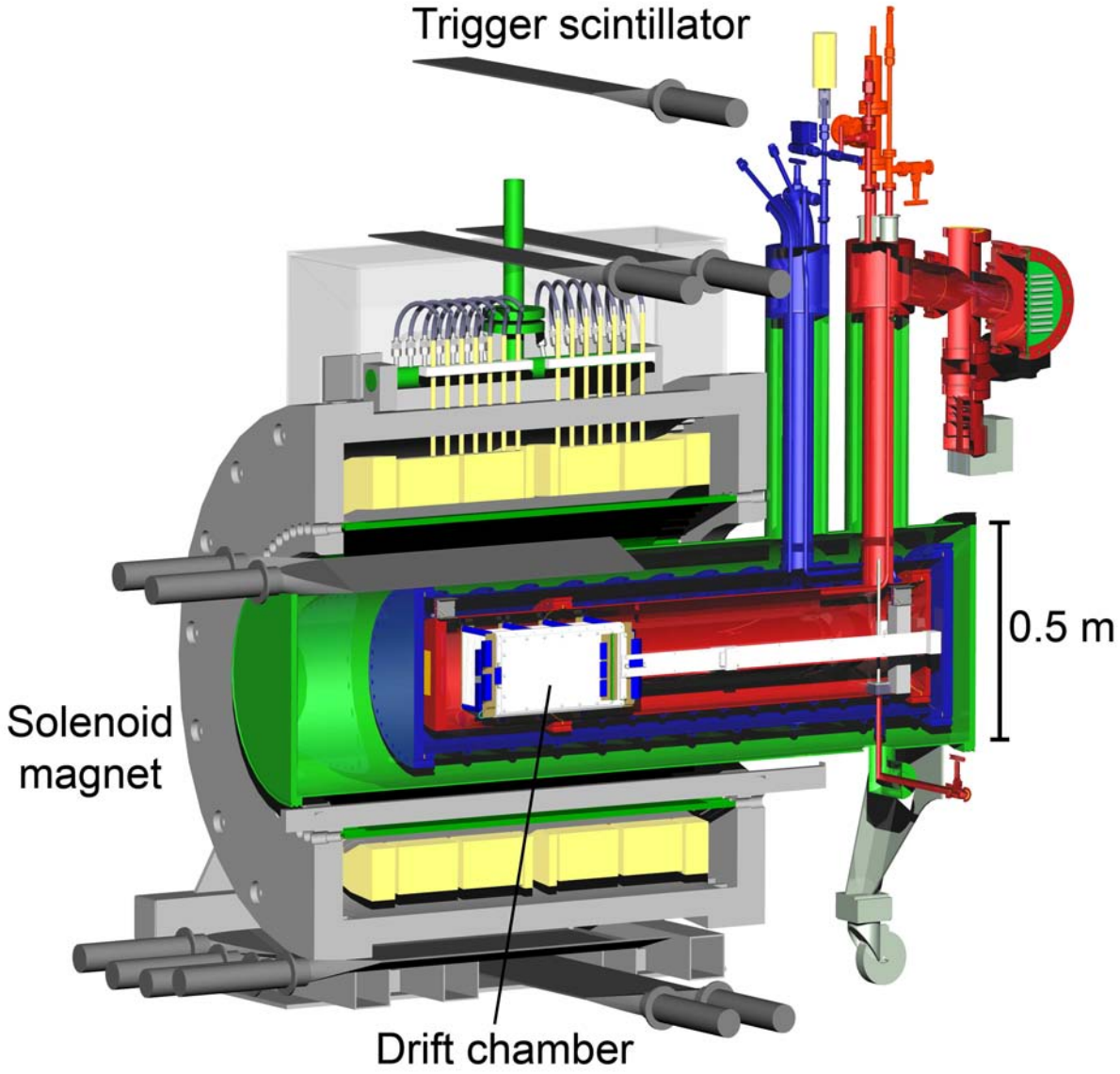

Figure 13. Global view of the experiment.

underneath the magnet as trigger counters for cosmic rays (see section 4.3). The temperature, the pressure and the level of both cryogenic liquids are monitored by the slow control sensors and the data are stored in a file (see section 4.4).

The commercial grade liquid argon is filled into the LAr container through a purification cartridge (see Figure 17) in order to reach a contamination of the LAr with electro-negative impurities of about 2 ppb (O_2 equivalent), which is necessary to obtain a lifetime of the drift electrons of the order of the maximal drift time, i.e., about 150 μs (see section 4.5). The LAr container is pumped before it is filled with LAr.

The experiment is located 11 m underground in a laboratory of the Institute for Particle Physics, ETH Zurich. The resulting underground depth of the

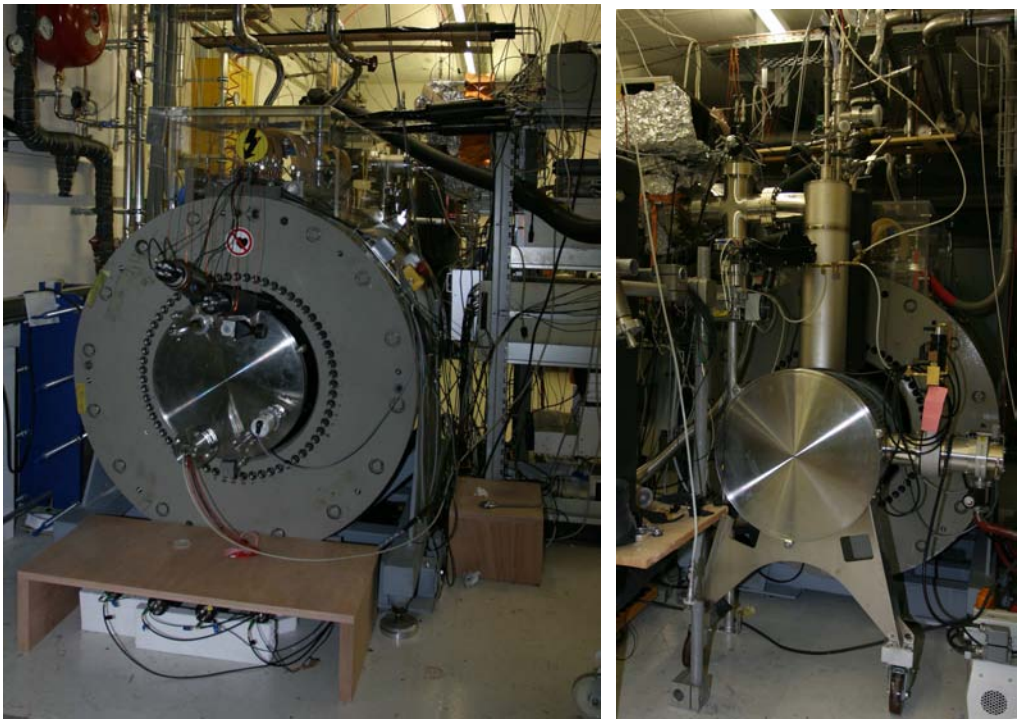

Figure 14. Pictures of the experiment taken from opposite sides.

chamber is 7.3 m water equivalent (730 g/cm^2).

4.1 The cryostat

The cryostat consists of three concentric cylinders (see Figures 5 and 13); it is constructed out of non–magnetic stainless steel (316L) in order not to distort the magnetic field. All the signal cables, the HV cables, slow control cables (and additional filling tubes) pass through vertical chimneys (80 mm inner diameter and about 500 mm long) welded on top of the LAr and LN_2 vessels at the end, which is outside the magnet (see Figure 13). A burst disk, safety valves and an electro–mechanical valve to regulate the nitrogen pressure were mounted on top of the chimneys.
The LAr vessel, containing the chamber, has an inner diameter of 250 mm and a total length of 1371 mm yielding a volume of about 65 ℓ of argon. The chamber is positioned in the cryostat such, that it is in the center of the magnet. The vessel is sealed on both ends with CF250 flanges. The liquid argon is filled and emptied through a 16 mm tube at the bottom of the vessel (see Figure 17).
The next concentric cylinder around the LAr vessel contains the liquid nitrogen bath. The absolute pressure is regulated to 2.7$\pm$0.1 bar in order to reach the boiling temperature of about 87 K for argon at 1 bar, hence preventing the freezing out of the LAr. Since the LAr vessel is hermetic (the over-pressure

valve opens at about 1.6 bar, well above the operating pressure of about 1 bar), the pressure of the argon is regulated only by its temperature, i.e., the temperature of the bath. The LN_2 cylinder is 1434 mm long and has an inner diameter of 350 mm with a volume of about 75 ℓ of LN_2. The technical grade LN_2 is contained in a dewar [9] with a total capacity of 180 ℓ at a pressure of 4.5 bar in order to fill the bath at 2.7 bar with a sufficient flux. During the data taking the LN_2 bath had to be refilled every 12 hours (see chapter 5).
The flanges of the LAr and the LN_2 vessels can be heated with two heating foils [10] with a power of 40 W per foil to speed up the warming process in case the containers have to be opened.
Both, the LN_2 and the LAr vessel, have to be vacuum insulated. The last concentrical cylinder serves as insulation vacuum chamber and has an outer diameter of 549 mm and a length of 1917 mm with an evacuated volume of about 220 ℓ. Also the vertical chimneys of the LN_2 and the LAr vessel are vacuum insulated up to the top. These two tubes and the whole LN_2 vessel are wrapped with about 40 layers of super–insulation foils to suppress the irradiated energy from the vacuum chamber (which is at room temperature). The insulation vacuum was better than 10^{-6} mbar with the cold cryostat.

4.2 The magnet

The solenoid magnet used in this experiment is the recycled SINDRUM I magnet from PSI. The bore holes in the end caps of the yoke were widened in order to have a 580 mm aperture to permit the insertion of the cryostat.
The magnet has a cylindrical shape with an outer diameter of the yoke of 1260 mm and a length of 1280 mm. The power supply delivers a maximal DC current of of 850 A at a voltage of 260 V; the power consumption of the magnet is about 220 kW for the maximal current. Table 2 summarizes the most important parameters of the magnet and its cooling system.

A field map was measured inside the LAr vessel, in the region of the drift chamber; it is shown in Figure 15. The current for these measurements was 800 A; the magnetic field reaches a maximum of 0.518 T in the center of the volume of the chamber and about 0.511 T at the side. Extrapolating linearly with the current, this corresponds to a field of 0.550 T in the center with a current of 850 A. The inhomogeneity of the field inside the chamber is of the order of 1.5 %.

[9] Air Liquide, type Ranger 180–15,5.
[10] MINCO Products, Inc. type HK5171R331L12.

External dimensions	Ø 1260 mm 1280 mm length
Weight	5.5 Tons
Internal dimensions	Ø 580 mm 1120 mm length
Magnetic field	0.55 T (at 850 A)
Homogeneity of the magnetic field	1.5 % inside the chamber
Max. current	850 A DC
Power consumption	220 kW at 850 A
Temperature difference at maximum power	40 °C

Table 2
Parameters of the SINDRUM I magnet.

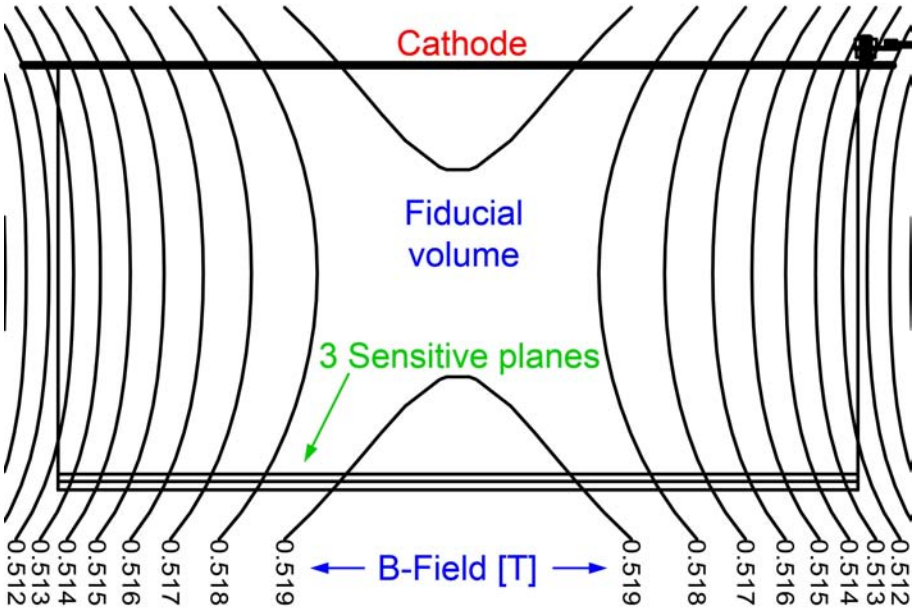

Figure 15. Map of the magnetic field in the time projection chamber. The map is drawn for a horizontal plane through the magnet axis, it has cylinder symmetry. The magnet current for the field measurements was 800 A (850 A is the maximal current).

4.3 The trigger system

There are a total of eleven trigger scintillators mounted as shown in Figure 13: three scintillators are on the top of the magnet, two are in the bore hole on

top of the cryostat and six are at the bottom of the magnet. The plastic scintillators measure 822 mm × 155 mm and are 5 mm thick; they are read out at one end by a Philips photomultiplier [11] tube.
The angular distribution of cosmic muons on the surface of the earth is proportional to $cos^2\theta_Z$ (θ_Z is the zenith angle), hence, most particles come from the zenith and the flux decreases with increasing zenith angle; this is even enhanced by the surrounding material of the detector. With a sensitive area of 0.045 m^2 and a solid angle acceptance around the zenith direction of 0.28 sr, the estimated muon rate is about 0.7 Hz [6]; this value is consistent with the measured trigger rate of 0.55 Hz. For stopping muons, the estimated rate corresponds to one event every 58 s, which is also compatible with the measured value.
The data were taken with two different triggers. The first one tiggers on through–going muons and requires a coincidence between the scintillators on top, in the bore hole and at the bottom of the magnet.
The second trigger was used to detect stopping muons. The V791 CAEN cards described in chapter 3 have an output of the amplified analog sum of all 32 channels. One analog sum of the module processing the signals from the central region of the collection plane was used for this trigger. The two scintillators in the magnet bore hole were used to open a gate; if a particle passes through the chamber the analog sum would be over a given threshold. The coincidence of the two signals generates a trigger at the end of the gate. The t_0 (passage of the particle through the chamber), used to determine the drift time, corresponds to the leading edge of the gate. Figure 16 shows the timing diagram for this trigger.

4.4 The slow control system

The slow control sensors are crucial to control the experiment during the critical phases, like the pumping period, the cooling down with LN_2 and filling LAr, and during the warming up; it is also important to monitor permanently the experiment during the data taking phase. The slow control sensors measure the temperature in many positions of the experiment, inside the liquid argon, around the cryostat and also in the cooling system of the magnet. Pressure gauges measure the argon and the nitrogen pressure and the capacitive level meters measure the level of the LN_2 and the LAr. All the data are read by a dedicated computer in a cycle of about 30 s and stored in a file (see [6] for more details).

[11] Philips, type XP2262.

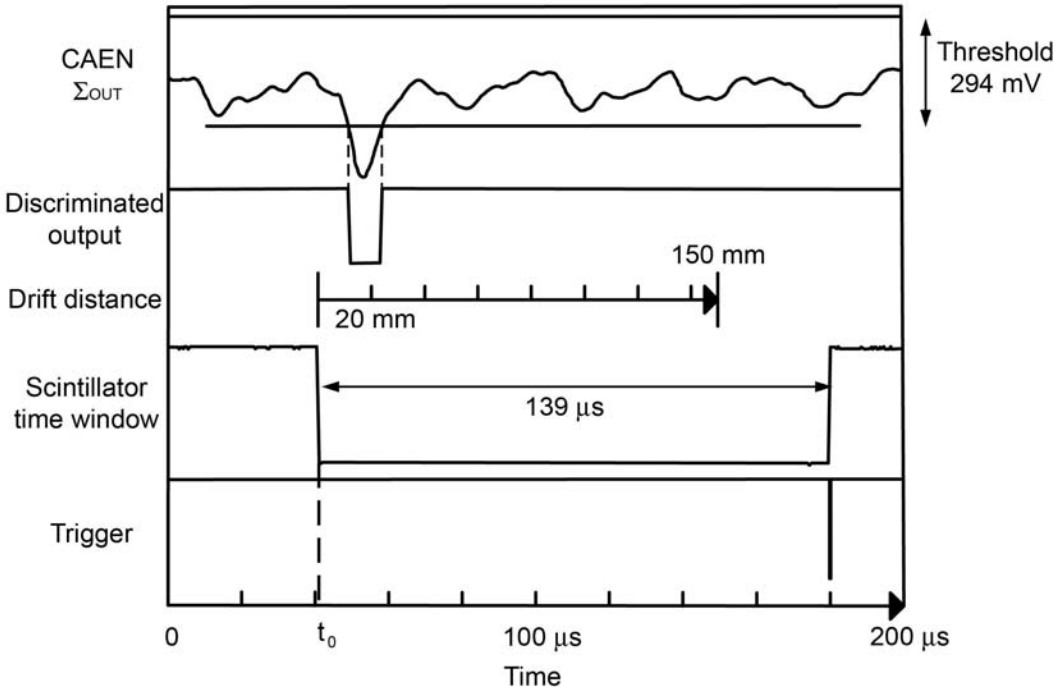

Figure 16. Timing diagram for the signals used to trigger on stopping muons. The trigger signal is synchronized with the scintillators, in oder to get the t_o needed to determine the drift time.

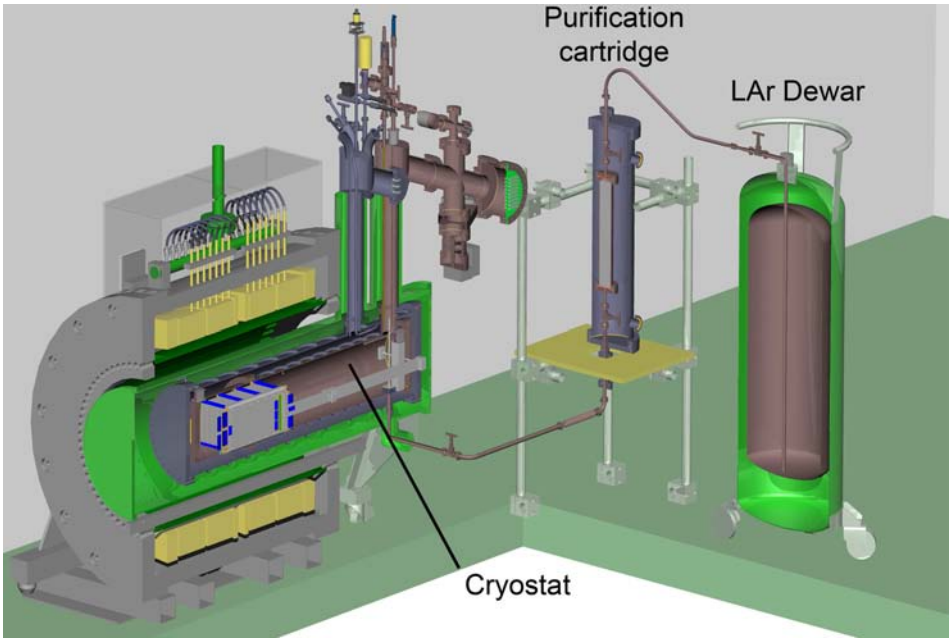

Figure 17. The setup with the LAr dewar and the purification cartridge used to fill the LAr vessel with the chamber.

4.5 Purification of the LAr during the filling

To reach an electron live time in liquid argon of 150 μs (corresponding to the maximal drift time in the chamber), the vessel and the chamber had to

be cleaned and evacuated to avoid electronegative impurities on the surfaces. Pumping the LAr vessel below $1 \cdot 10^{-4}$ mbar guarantees a purity better than 1 ppb of residual oxygen. In our case, the chamber and the cables were pumped to $5 \cdot 10^{-6}$ mbar.
The commercial liquid argon 46 [12] has a declared content of $O_2 < 5$ ppm and $H_2O < 10$ ppm and there is no commercially available argon with a purity of the order of ppb. Thus, a filter for electronegative ions has been placed between the dewar with the commercial LAr and the vessel with the chamber as shown in Figure 17.
The filter consists of a cylinder with 63 mm internal diameter and 463 mm length made of stainless steel, filled with fine (grain size $\approx 5\,\mu$m) copper powder. On both ends of the tube there are metal sieves with $\approx 3\,\mu$m holes in order to contain the powder inside the cartridge. The small amount of oxygen content in the liquid argon will be bound chemically by the copper in the cartridge via the $2Cu + O_2 \rightarrow 2CuO$ reaction. At 87 K the water inside the LAr is trapped on the surface of the powder and is easily filtered.
The cartridge is enclosed by an insulated cylinder of 200 mm inner diameter and 898 mm length. Before filling with LAr, the cartridge is cooled by inserting LN_2 into this cylinder.
The cartridge was first filled with copper oxide (CuO) purchased from Fluka [13] and then reduced by flowing a hydrogen/argon gas mixture at about 200 °C through the closed cartridge; the chemical reaction of the reduction process is $CuO + H_2 \rightarrow Cu + H_2O$. The admixture of argon gas avoids an overheating due to the reaction and the temperature can be controlled by varying the argon percentage, it also helps the water vapor to be expelled.

5 Test run with cosmic rays

In November 2004 the setup was ready for a first test. Starting with the vacuum pumping of the liquid argon vessel, the slow control program stored all important information on the status of the setup in a completely automatic way.

5.1 Vacuum in the cryostat

The liquid argon vessel with the chamber installed was pumped the first time in May 2004 to test the vacuum tightness of the vessel and to let the cables (with a total length of about 3 km) out-gas. In the next month the vessel was kept

[12] Purchased from Carbagas AG
[13] Fluka, Cupric oxide, puriss, p.a. $\geq 99\%$

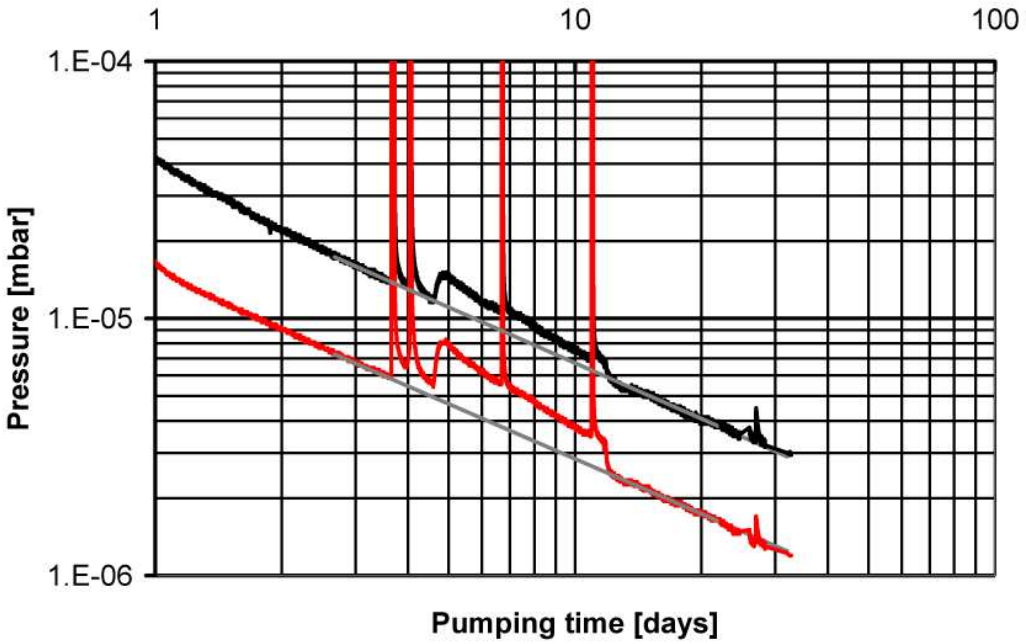

Figure 18. Pressure measurements with two vacuum gauges on the LAr cryostat during the pumping period of a month. The pressure near the drift chamber in the cryostat should be between the two measurements. The zero point of the time coordinate corresponds to the 16^{th} of September 2005 (see text).

as much as possible under vacuum or under argon or dry nitrogen gas to avoid that the cables and the cryostat surfaces absorbed water. The pressure reached shortly before the liquid argon filling was better than 5×10^{-6} mbar, well below the requirement. In Figure 18 the pressure during the period from the 16^{th} of September until the 19^{th} of October 2004 is shown. During this pumping period, two vacuum gauges mounted on the LAr vessel were read: one near the turbomolecular pump, the other one was mounted on the filling tube, at the bottom of the vessel; the pressure near the drift chamber should be between the two values. The four spikes seen in the figure correspond to vacuum breaks with Ar gas in order to finish the mounting. The vacuum breaks had no influence on the final vacuum, and after a few hours the equilibrium with the out-gassing was reached again. Around day 5 until day 11 the temperature of the vessel was slightly increased up to about 35 °C, as a consequence, the out-gassing rate and the pressure increased. After this period the temperature returned to room temperature of about 21 °C.

The pressure reached 1×10^{-6} mbar with the cryostat at room temperature and 1×10^{-7} mbar with the liquid nitrogen vessel filled, due to the big cold surface acting as a cryogenic pump for water.

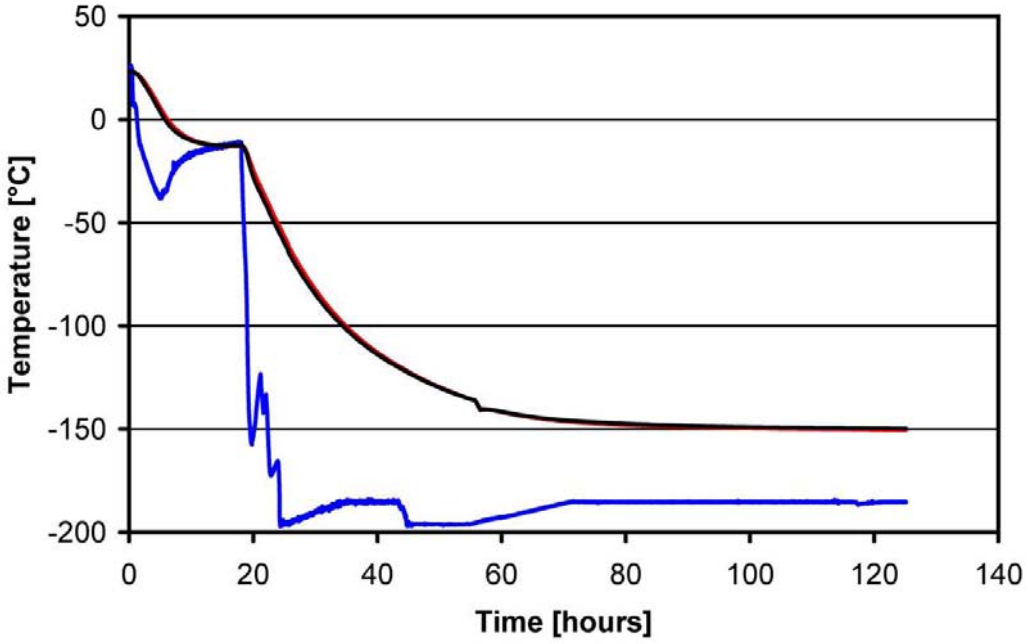

Figure 19. Temperature at the bottom of the LAr cylinder (blue), on the drift chamber frame (red) and the ambient temperature in the LAr vessel (black) during the cooling down period.

5.2 Cooling down and filling with liquid argon

In November 2004 the liquid nitrogen vessel was cooled down slowly by filling small amounts of liquid nitrogen distributed over a period of about two days; the LAr vessel was still under vacuum during this phase. The filling rate was chosen in order to keep the temperature of the drift chamber as homogeneous as possible. Figure 19 shows the temperature at three different locations: at the bottom of the LAr cylinder (blue), on the drift chamber frame (red) and the ambient temperature in the LAr vessel (black); the latter two temperatures are almost indistinguishable on Figure 19. The difference between the temperature of the drift chamber frame and the ambient temperature in the LAr vessel is shown in Figure 20; the liquid nitrogen filling rate was chosen in order not to exceed a maximal difference of 4 °C.

Once the LN_2 vessel was filled with liquid nitrogen, the pressure was regulated (see chapter 4) to an absolute pressure of 2.7 bar (in order to reach the right temperature for liquid argon with an absolute pressure of about 1 bar), and the LAr container was filled ($\sim 65\,\ell$) in about 2 hours.

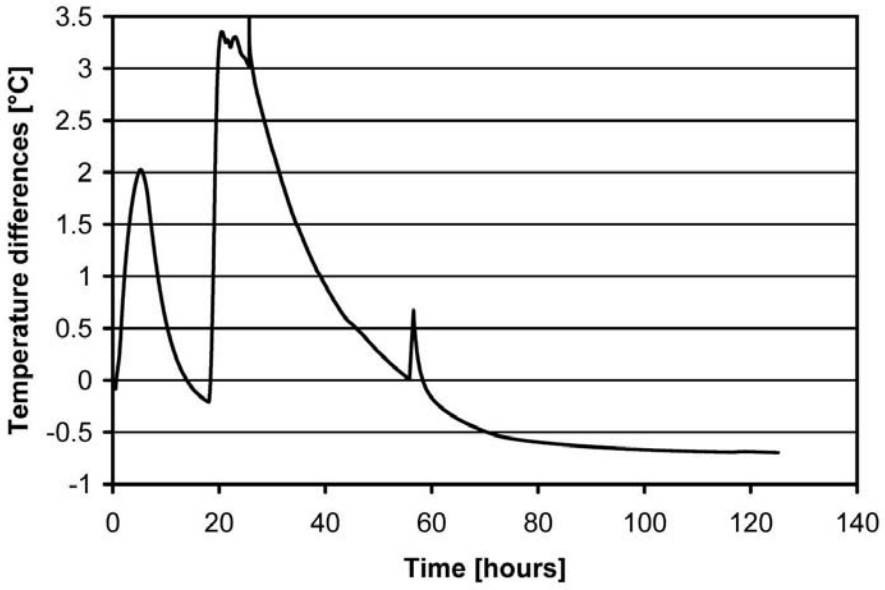

Figure 20. Difference between the temperature of the drift chamber frame and the ambient temperature in the evacuated LAr vessel during the cooling down period.

5.3 Measurements with the LAr TPC

On November 23^{rd} 2004 the setup was ready for a first test. Starting the tests without magnetic field and triggering with the scintillator counters, clean cosmic ray tracks were immediately observed at a drift field of 500 V/cm. With every run 100 trigger events were stored. At the beginning there was a commissioning period without magnetic field, when some through–going muon events were taken with increasing drift field. The maximum field applied was 1.5 kV/cm, i.e., 22.5 kV at the cathode. After a week of operation, breakdowns occurred in the high voltage system. After this time the high voltage was limited to 4.7 kV, corresponding to a drift field of 0.3 kV/cm.
The level of the liquid nitrogen was monitored to avoid a drop to a too low level, which would cause an increase of the temperature in the liquid argon vessel. A re-filling every 12 hours was necessary to replace the evaporated nitrogen, corresponding to a global consumption of about 1.4 ℓ/h, equivalent to 62 W of thermal losses. Figure 21 shows the LN_2 level and the temperature and pressure of the liquid argon during two days of data taking with the visible liquid nitrogen fillings twice a day.

In the beginning of the test run a coincidence of the scintillators was required for a trigger to detect through–going muons. In this case only about 20 – 30 % of the triggered events had a track in the drift chamber. This efficiency is given by the position of the scintillators, which give a trigger signal also for muons passing close to the chamber, but not traversing the sensitive volume. To trigger on stopping muons, a coincidence between the scintillators on top

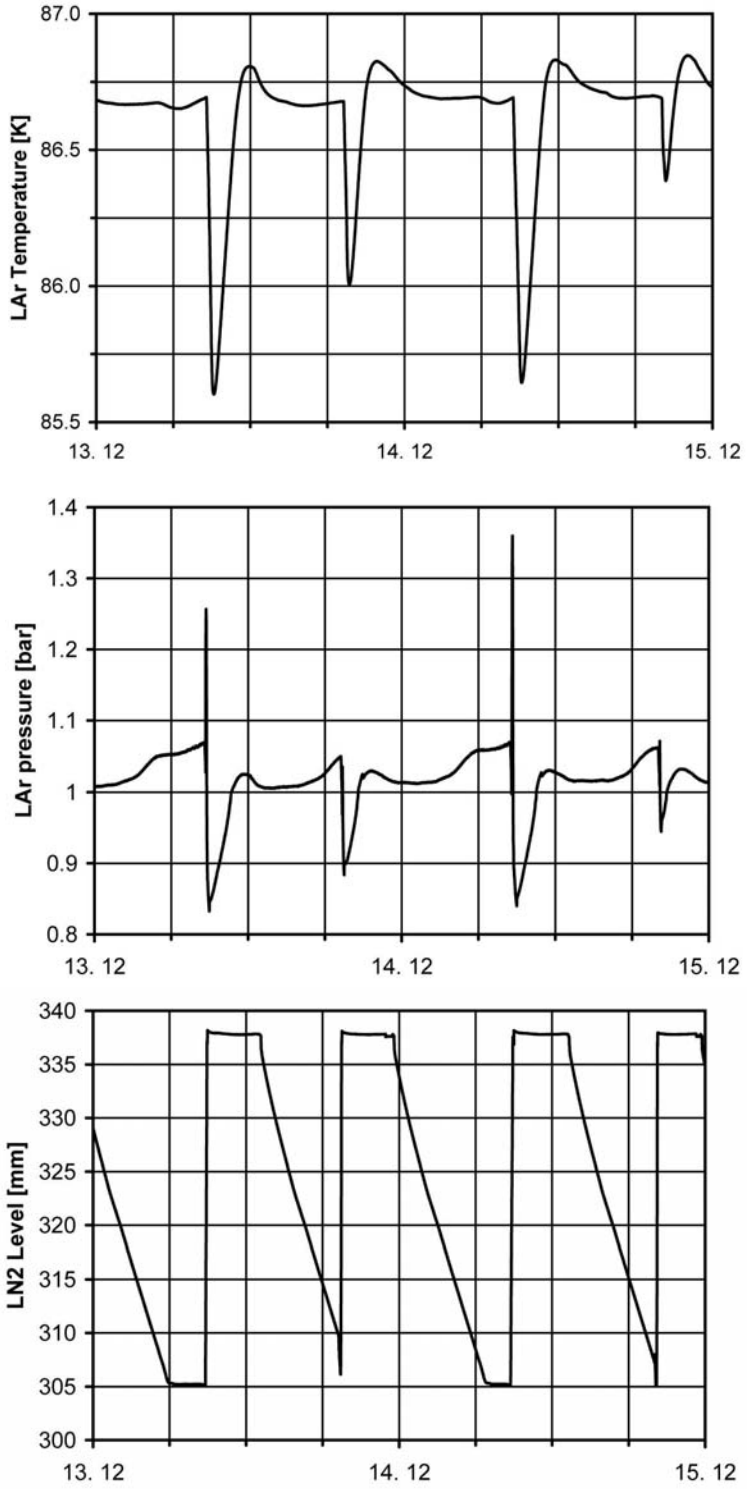

Figure 21. LN_2 level and the temperature and pressure of the liquid argon during two days of data taking. Visible are the liquid nitrogen fillings twice a day.

of the cryostat in the magnet bore hole and the analog sum output of the 32 channels from a CAEN V791 board was required. The scintillators give in this case only the t_0 time of the event, needed to determine the drift time.

Figures 22 shows some examples of visually selected events from the total sample of $\sim$30 400 collected events. The raw data from the collection plane are displayed as two-dimensional projection of tracks in the plane perpendicular to the magnetic field: the horizontal axes correspond to the drift time (converted to a drift distance with the drift velocity) with a full scale of about 150 mm, and the vertical axes are the strip number coordinates, also with a full scale of 150 mm. The magnetic field is pointing into the plane of the figure and had a value of 0.55 T. The events are interpreted as a) a reaction with an argon nucleus, b) a stopping positive muon with the decay positron, c) a muon track with an electron–positron pair, d) a muon with a δ–electron, e) a stopping negative muon and f) an electro-magnetic shower.

6 Event selection and results

For a first analysis events with a simple topology, namely positrons emitted by stopped muons and δ-electrons from passing–through muons were chosen [20]. The collected events were scanned by eye with the Qscan program. This program displays a two dimensional gray scale representation of the output signal in the wire/drift time coordinate plane and provides the possibility to call a hit finding and fitting algorithm, which gives the needed information for the event reconstruction. Events were selected if the track length of the electron/positron (in the plane perpendicular to the magnetic field) is at least 2 cm and if the curvature of the track is well visible, i.e. the transverse projected track should be recognizable as a section of a circle, which biases the event selection.
A 3D reconstruction of the electron/positron tracks is necessary for a full calorimetric reconstruction and a determination of the total momentum. A detailed description of the spatial reconstruction procedure is given in [3,7].

A small sample of 15 δ-electrons and 9 decay positrons, fully contained in the chamber, were selected from 30'400 recorded and scanned events. These events were reconstructed and their momentum and kinetic energy was determined from the magnetic bending and the summed up energy loss, respectively [20]. In Figures 23 and 24 the transverse momentum obtained from the energy (charge) measurement is plotted against the momentum from the magnetic bending for δ-electrons and decay positrons together (circles: δ-electrons, triangles: decay-positrons). The straight line fit (fit function: $y = p1 \cdot x$) through the data points is also shown. In Figure 23 no errors were assigned to the individual data points and Figure 24 includes the errors of the transverse mo-

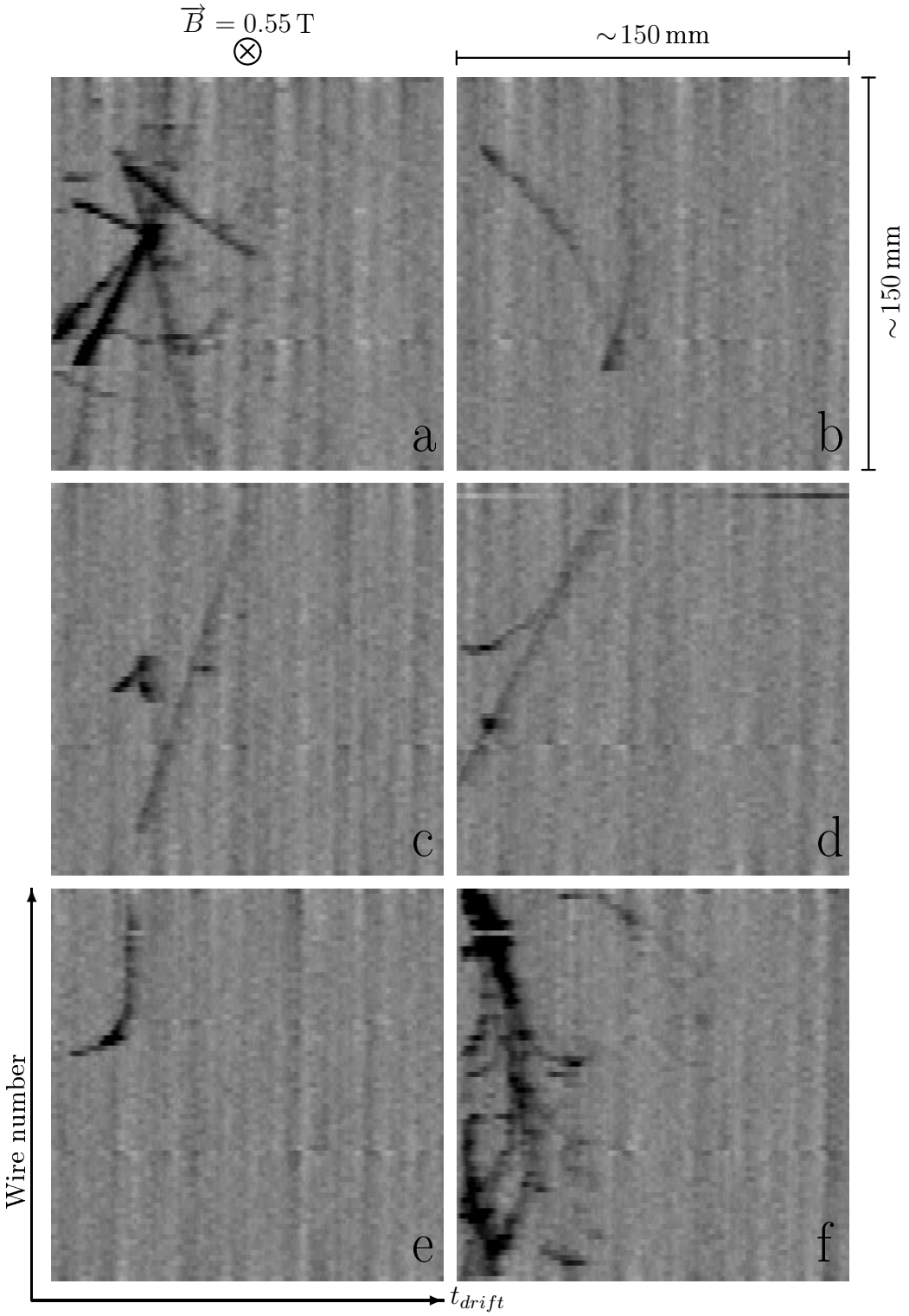

Figure 22. Six examples of real events collected with the liquid Argon TPC prototype immersed in a magnetic field of 0.55 T. The horizontal axes correspond to the time coordinate and the vertical axes are the wire coordinate, both correspond to a full scale of 150 mm.

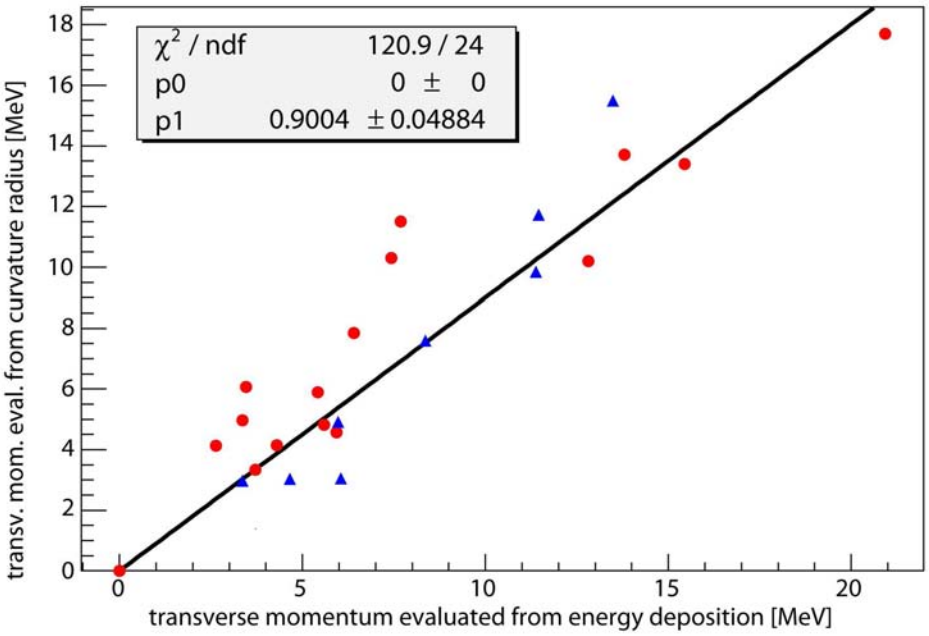

Figure 23. Correlation between the two momentum measurement methods for δ-electrons (circles) and decay-positrons (triangles)

mentum due to multiple scattering estimated according to equation 12. These errors are obviously much larger than the scattering of the data points around the fitted straight line; the χ^2/ndf is equal 0.05, indicating that the error is over estimated. This discrepancy can be attributed to the event selection, introducing a bias towards tracks with little multiple scattering showing nicely bent tracks. For the error of the transverse momentum evaluated from the energy see [20].
The slopes of the two plots are p1=0.9480± 0.0431 for Figure 23, and p1=0.9122 ± 0.1814 for Figure 24; thus, the slopes are compatible with 1.

6.1 Energy loss and the electron lifetime in LAr

Figure 25 shows the measured kinetic energy plotted versus the path length. The slope of a linear fit gives an estimate for the (average) specific energy loss dE/dx, since the energy loss is assumed to be constant (except for the last 2 mm of a track [20]). The slope in Figure 25 corresponds to an average energy loss of 1.642 (± 0.069) MeV/cm. The theoretically expected value is about 1.9 - 2.2 MeV/cm for electrons (positrons) in the range between 1 MeV and 20 MeV. Thus, the measured and the expected values differ by about 20%. However, the energy loss dE/dx from the measured charge depends on the assumed lifetime τ of the drift electrons; a first estimate of 150 μs was used for the lifetime to calculate the kinetic energy. Varying the electron lifetime and recalculating

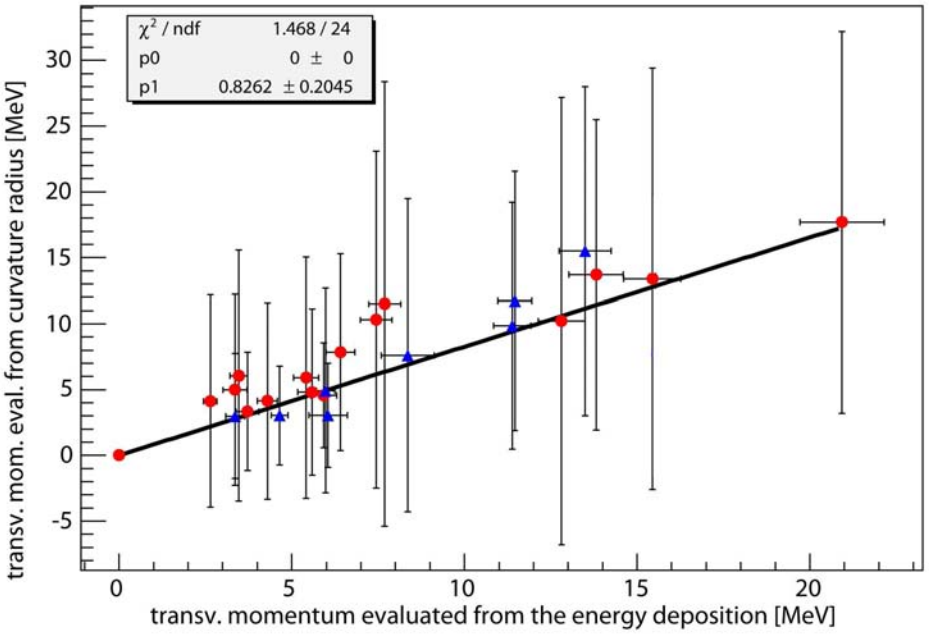

Figure 24. Correlation between the two momentum measurement methods for δ-electrons (circles) and decay-positrons (triangles) with an error estimation due to multiple scattering

the kinetic energy of all events, the comparison of the average dE/dx with the expected theoretical value yields an electron lifetime in the range of 60 μs - 80μs.

7 Conclusions

In an effort to further develop the LAr TPC technology, a small test TPC was built and operated for the first time in a magnetic field (0.55 T), which was perpendicular to the electric drift field. The quality of cosmic ray tracks is not significantly decreased with the magnetic field turned on.

Combining the excellent imaging and calorimetric properties of a LAr TPC with a magnetic field opens new experimental possibilities. The magnetic bending of charged particles allows the momentum determination also for particles leaving the sensitive volume and the determination of the sign of the electric charge. The latter feature is a must in future neutrino experiments searching for CP–violating effects in the lepton sector.

A special interface between the ICARUS front-end electronics (V791 CAEN boards) and the computer was developed and built for the data acquisition

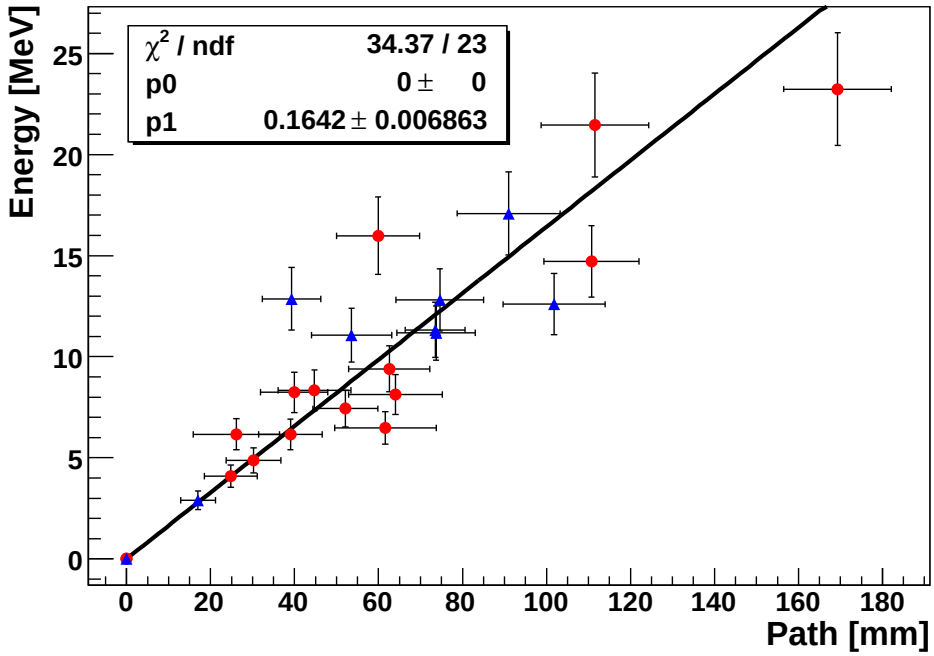

Figure 25. Measured energy as a function of the reconstructed path length of the δ-electrons (circles) and the decay-positrons (triangles)

system of this experiment. It is able to store the continuous flow of digital data in a circular buffer and to send the data to the PCI card in the computer, once a trigger has occurred. The buffer size is large enough to store the digitized data of all the channels for a time interval corresponding to the maximal drift time occurring in the chamber.

A small sample of selected δ-ray and muon decay events were analyzed, showing that the momentum of an electron (positron) determined from the magnetic bending and from its kinetic energy are consistent for these events. The kinetic energy was calculated from the measured ionization charge, summed along the whole track.

Acknowledgements

We thank PSI for lending us the SINDRUM I magnet with the power supply and ETH Zurich to provide us with the necessary infrastructure to operate the magnet at ETHZ. We are also indebted to the INFN Padova group who kindly lent us the readout electronics; especially we thank Sandro Centro (INFN, Padova) for his support. We thank P. Picchi and F. Pietropaolo for useful discussions. This work was supported by ETH Zurich and the Swiss National Science Foundation.

References

[1] C. Rubbia, *The Liquid-Argon Time projection Chamber: a new concept for Neutrino Detector*, CERN-EP/77-08, (1977).

[2] ICARUS Collaboration, *A second-Generation Proton Decay Experiment and Neutrino Observatory at the Gran Sasso Laboratory*, LNGS-P28/2001.

[3] S. Amerio et al., Nucl. Instr. and Meth. A 527 (2004) 329.

[4] A. Rubbia, arXiv:hep-ph/0407297.

[5] A. Badertscher, M. Laffranchi, A. Meregaglia and A. Rubbia, New J. Phys. **7**, 63 (2005) [arXiv:physics/0412080].

[6] M. Laffranchi, PhD thesis No. 16002, ETH Zurich, March 2005, available at http://neutrino.ethz.ch/diplomathesis.html.

[7] J. Rico, PhD thesis No. 14906, ETH Zurich, November 2002, available at http://neutrino.ethz.ch/diplomathesis.html.

[8] E. Buckley et al., Nucl Instr. and Meth. A 275 (1989) 364.

[9] A. Bettini et al., Nucl Instr. and Meth. A 305 (1991) 177.

[10] F. Sauli, CERN 77-09, May 1977.

[11] S. Amoruso et al., Nucl. Instr. and Meth. A 516 (2004) 68.

[12] A. Rubbia, arXiv:hep-ph/0106088.

[13] A. Rubbia, arXiv:hep-ph/0402110.

[14] A. Bueno, M. Campanelli, S. Navas-Concha and A. Rubbia, "On the energy and baseline optimization to study effects related to the Nucl. Phys. B **631**, 239 (2002) [arXiv:hep-ph/0112297].

[15] D.B. Cline et al., Nucl. Instr. and Meth. A 503 (2003) 136.

[16] Review of Particle Physics, Phys. Lett. B 592 (2004).

[17] Technical Information Manual available at www.caen.it/Products/Front End/VME/Read-Out Liquid Argon TPC detector.

[18] S. Centro et al., Nucl. Instr. and Meth. A 409 (1998) 300.

[19] P. Horowitz and W. Hill, *The Art of Electronics, 2. ed.*, Cambridge University Press, UK, 1993.

[20] A. Müller, Diploma thesis, ETH Zurich, March 2005, available at http://neutrino.ethz.ch/diplomathesis.html.